Comparative static structural assessment of an energy-efficient prototype vehicle chassis using finite element analysis: AISI 1020 steel vs. 6061-T6 aluminum

Muhammad Fadil Andira*, Wanda Afnison, Waskito and Delima Yanti Sari

Department of Mechanical Engineering, Faculty of Engineering, Universitas Negeri Padang, **Indonesia**

*Corresponding Author: wandaafnison@ft.unp.ac.id

Received: 08 July 2025; *Revised:* 24 October 2025; *Accepted:* 30 October 2025

https://doi.org/10.58712/jerel.v4i3.199

Abstract: This study evaluates the static structural performance of a Prototype-class energy-efficient vehicle chassis for the Indonesian *Kontes Mobil Hemat Energi* (KMHE; Energy-Efficient Car Competition) by comparing two material options, AISI 1020 carbon steel and Al 6061-T6, under a consistent load representation. Three-dimensional chassis models were developed in SolidWorks and assessed using static finite element analysis (FEA). The loading scenario included gravitational body force and two concentrated static loads representing operational conditions: 700 N applied at the driver seat region and 300 N applied at the engine mounting area. A curvature-based meshing strategy was adopted, with element sizes ranging from 1.6 to 8 mm, resulting in approximately 1,700,093 nodes to capture geometric details in joints and curved members. The AISI 1020 chassis produced a maximum von Mises stress of 278.6 MPa concentrated near the engine mounting joint, a maximum total deformation of 2.1 mm in the roll-bar region, and a minimum factor of safety of 1.3. In contrast, the Al 6061-T6 chassis exhibited a lower peak stress of 61 MPa at the rear wheel mounting region, a higher deformation of 3.4 mm at the roll bar, and a factor of safety of 4.5. The findings confirm a trade-off between stiffness and safety margin: steel offers higher stiffness but an insufficient safety margin, while aluminium significantly improves the static safety margin with increased deformation. These results provide design guidance for reinforcing critical regions and enhancing the robustness of competition-ready chassis.

Keywords: vehicle chassis; finite element analysis; von Mises stress; total deformation; lightweight structures

1. Introduction

Over the past decades, advances in automotive engineering have substantially improved vehicle design and performance, particularly in the light-vehicle segment (Cornet et al., 2023; Czerwinski, 2021; Laveneziana et al., 2025). Light vehicles, such as pickup trucks, compact SUVs, and vans, remain widely adopted due to their versatility for both daily mobility and cargo transport (Zhu et al., 2023). A key driver of this adoption is the use of diesel powertrains, which are recognized for high torque output, durability, and superior fuel efficiency relative to gasoline engines. Nevertheless, diesel engines typically impose greater mass and different load characteristics on the vehicle structure, thereby increasing the structural demands on the chassis (Anil et al., 2025; Zamzam et al., 2025). As a result, modern chassis development must continuously address a fundamental engineering trade-off: achieving adequate strength and durability while minimizing weight, maintaining vehicle performance, and ensuring occupant comfort and safety. These objectives also align with broader environmental goals, as improved structural efficiency supports reduced fuel consumption and emissions. In Indonesia, initiatives such as the *Kontes Mobil Hemat Energi* (KMHE; Energy-Efficient Car Competition) have further accelerated research and development of energy-efficient vehicles in both Urban and Prototype categories (Brown et al., 2022; Golinska-Dawson & Sethanan, 2023; Razmjoo et al., 2021), encouraging design decisions that prioritize lightweight construction without compromising safety and reliability.

For Prototype-class energy-efficient vehicles, the chassis is a critical load-bearing component that must be simultaneously strong and lightweight. Material selection and structural configuration directly influence stiffness, stress distribution, and the resulting factor of safety (Liu et al., 2024; Muayad et al., 2025; Tuninetti et al., 2025). Finite Element Analysis (FEA) has become a standard approach for evaluating chassis performance because it enables engineers to quantify von Mises stress (Quang, 2019), total deformation, and safety factors under representative loading scenarios, thereby identifying critical regions that may lead to failure or unacceptable deflection. Despite the widespread use of FEA in chassis development, many existing studies and student competition designs emphasize general stress deformation evaluation without providing a systematic comparison of candidate materials under the same chassis geometry and static load representation, particularly for Prototype vehicles that integrate diesel internal combustion engines (Gadola et al., 2019; Lagaros et al., 2022). In addition, a practical gap remains in translating FEA findings into a clear design-improvement direction: where the critical stress paths are located, how close the structure is to yielding, and what material choice most effectively increases safety margin while maintaining acceptable stiffness for the driver compartment and key structural members.

Preliminary analysis of the initial Prototype chassis design considered in this study indicates a maximum von Mises stress of 278.6 MPa, approaching the yield strength of the selected material (3.516×10^8 N/m²). This result suggests that specific structural regions experience excessive loading and may be susceptible to plastic deformation or permanent damage if the design is used without modification. The displacement analysis further shows a maximum deflection of 2.132 mm in the driver's roll bar region, indicating potential geometric changes in critical areas. These concerns are reinforced by the minimum factor of safety of 1.3, which is below commonly recommended values (approximately 2.5–4.0) for vehicle structures exposed to uncertainties, variability in loading, and operational conditions. Collectively, these findings highlight that the current chassis configuration has insufficient safety margin and requires improvement to satisfy expected structural robustness (Ding et al., 2025; Kabashi et al., 2025; Silva et al., 2024).

Accordingly, this research addresses the identified gap by conducting a comparative static structural assessment of two material alternatives, AISI 1020 steel and 6061-T6 aluminum, applied to the chassis of an energy-efficient Prototype vehicle. The novelty of this work lies in providing a consistent, geometry-controlled comparison of stress response, deformation behavior, and safety margin between a conventional steel option and a lightweight aluminum alloy option under the exact static loading representation of driver and engine masses, using a curvature-based meshing strategy to improve element quality in complex chassis features. The primary objective of this study is to evaluate whether a material substitution strategy can significantly increase the chassis safety factor while maintaining acceptable deformation levels in critical regions. The research contribution is twofold: (1) it delivers quantitative evidence supporting material-driven improvements in chassis safety and structural performance for Prototype energy-efficient vehicles, and (2) it offers design-relevant insights on stress concentration and stiffness-sensitive regions to guide future chassis optimization toward safer and more reliable competition-ready prototypes.

2. Methods

This study evaluates the static structural performance of a chassis developed for an energy-efficient vehicle competition (KMHE prototype class). Prototype vehicles typically use compact dimensions and a three-wheel configuration; therefore, the chassis must achieve an appropriate balance between low mass and structural integrity to ensure driver safety. The methodology combines 3D CAD modeling and finite element analysis (FEA) to compare two chassis designs manufactured from different materials, with emphasis on stress distribution, total deformation, and safety factors.

2.1 Chassis design selection and material choice

The chassis geometries were selected to comply with the KMHE prototype regulations and to

accommodate the driver position, engine placement, and other key vehicle components. Two chassis variants were evaluated using different structural materials: AISI 1020 carbon steel and Aluminum 6061-T6. These materials were selected for their everyday use in lightweight vehicle structures and their distinct mechanical properties, which enable a direct assessment of how material selection influences stiffness, strength, and deformation behavior (Demiral, 2025; Sarvestani et al., 2025). The geometric dimensions of both chassis and the mechanical properties used in the simulations are summarized in Tables 1–2 and serve as the baseline inputs for the FEA.

Table 1. Chassis dimensional specifications

Chassis type	Crumple zone (mm)	Wheelbase (mm)	Width (mm)	Length (mm)
AISI 1020	100	1500	532	2256
Al 6061-T6	100	1000	900	2500

Table 2. Material poperties

Property	AISI 1020	Al 6061-T6
Elastic modulus	200000 N/mm^2	69000 N/mm^2
Poisson's ratio	O,29 N/A	O,33 N/A
Shear modulus	77000 N/mm^2	0,85 N/A
Mass density	7900 Kg/m^3	2700 Kg/m^3
Tensile strengh	420,507 N/mm^2	310 N/mm^2
Yiel strength	351,571 N/mm^2	275 N/mm^2

2.2 3D modeling

Both chassis concepts were developed as detailed three-dimensional CAD models using SolidWorks to support subsequent structural evaluation and comparison. The modeling process was carried out under the dimensional constraints and packaging requirements defined by the prototype class regulations to ensure geometric compliance and functional feasibility (Ambaw et al., 2022; Pign`eres et al., 2025). Key layout elements, such as the driver cockpit envelope, engine and drivetrain mounting location, and the arrangement of primary and secondary structural members, were incorporated to represent realistic vehicle architecture and load paths. This approach ensured that the resulting frame geometries were not only manufacturable but also representative of actual operating conditions. The finalized CAD configurations of the first and second chassis are presented in Figure 1.

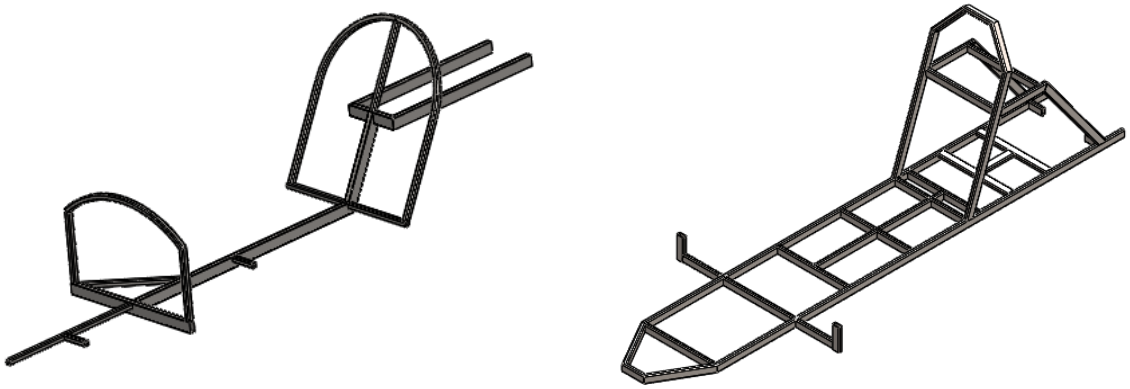

(a) First chassis (b) Second chassis

Figure 1. Chassis configurations

2.3 Load

In the gravity-loading analysis, the chassis frame was subjected to a uniform gravitational body force to represent the structure's self-weight and establish a baseline loading condition for the numerical simulation. A gravitational acceleration of 9.81 m/s² was applied in the negative vertical direction to all structural members, enabling the determination of the frame's mass distribution and the corresponding center of gravity location. This step is essential for verifying the vehicle's stability characteristics and for providing realistic initial conditions before additional operational load cases. The applied gravitational loading and the resulting load direction acting on both chassis configurations are illustrated in Figure 2.

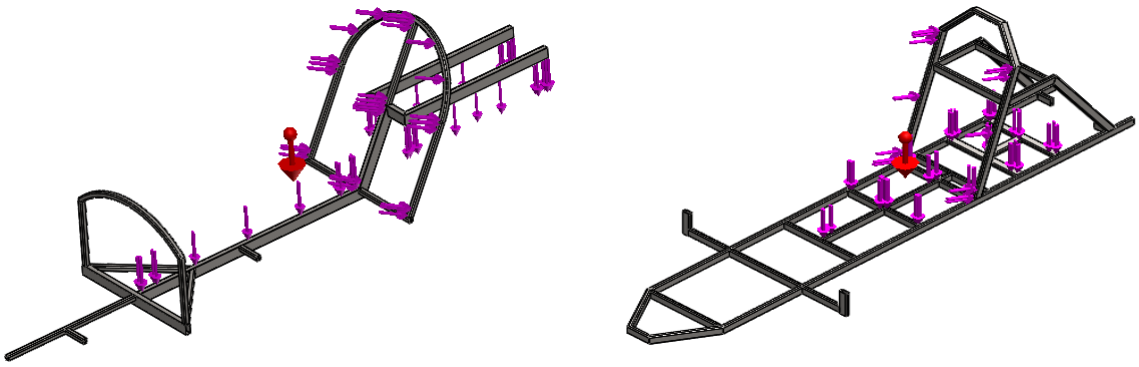

(a) First chassis (b) Second chassis

Figure 2. Direction of the gravitational load acting on the chassis frame

In this loading case, a concentrated vertical load of 700 N was applied at the driver's seat region to represent the combined weight of the driver and the associated safety equipment under operating conditions. The load was imposed in the downward direction and transferred through the seat mounting points to the surrounding frame members, thereby reproducing the primary occupant-induced force path experienced during everyday vehicle use. This scenario is critical for evaluating the local stiffness and global structural response of the chassis, particularly in the cockpit area, where bending and stress concentrations are commonly observed. The applied driver-weight loading condition for both chassis configurations is illustrated in Figure 3.

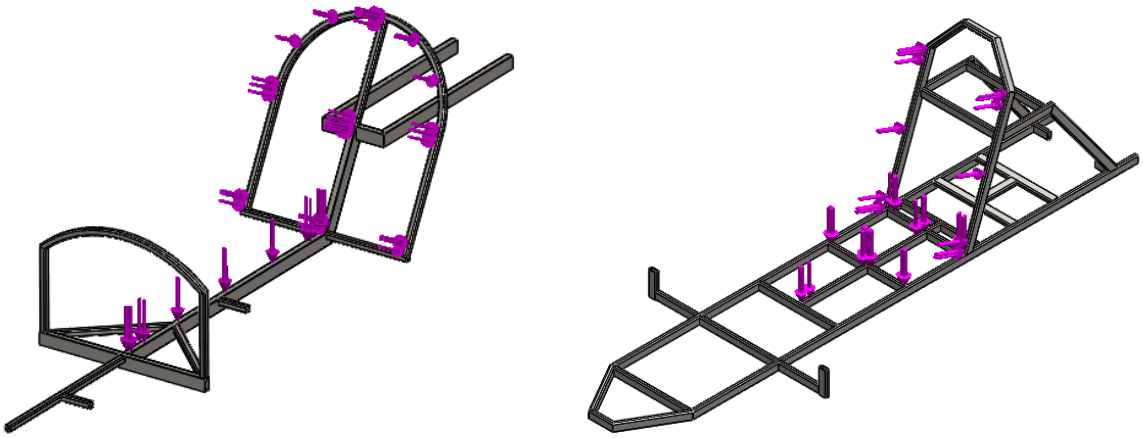

(a) First chassis and (b) Second chassis

Figure 3. Driver weight loading (700 N) applied to the chassis frame

In this loading scenario, a vertical static load of 300 N was applied at the engine mounting region to represent the gravitational effect of the powertrain mass on the chassis during steady-state operation. The load was imposed in the downward direction and distributed through the mounting points to the adjacent frame members, thereby replicating the primary load transfer mechanism from the engine to the chassis structure. Including this load case is essential for assessing the structural integrity and stiffness of the rear (or powertrain) section of the frame, where localized bending, joint stresses, and potential deformation can occur due to concentrated masses. The applied engine-weight loading configuration for both chassis designs is presented in Figure 4.

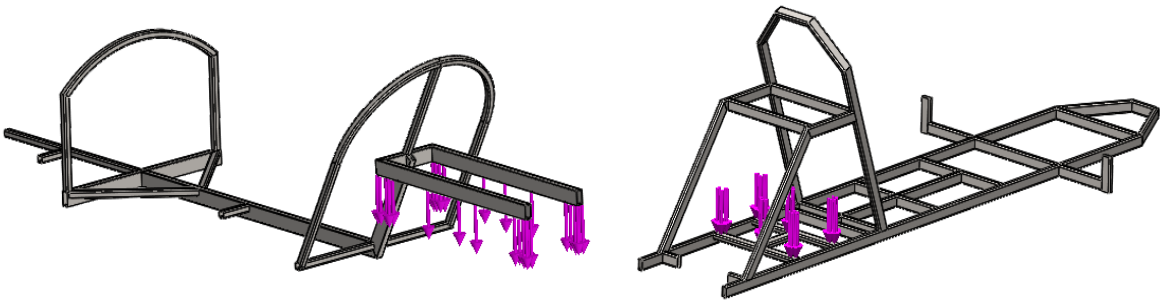

(a) First chassis (b) Second chassis

Figure 4. Engine weight loading (300 N) applied to the engine mounting area

2.4 Mesh

In this study, the finite element discretization was generated using a curvature-based meshing strategy to accurately capture geometric variations, particularly in regions with bends and joints, while maintaining computational efficiency. The mesh was defined with a maximum element size of 8 mm and a minimum of 1.6 mm, resulting in 1,700,093 nodes for the chassis model. These mesh parameters were adopted based on prior work, which showed they provide a suitable balance between numerical accuracy and simulation cost, producing stable and reliable results without excessive computation time (Heidari et al., 2024; Nozari et al., 2025). The meshing configuration and boundary-condition locations for both chassis designs are shown in Figure 5.

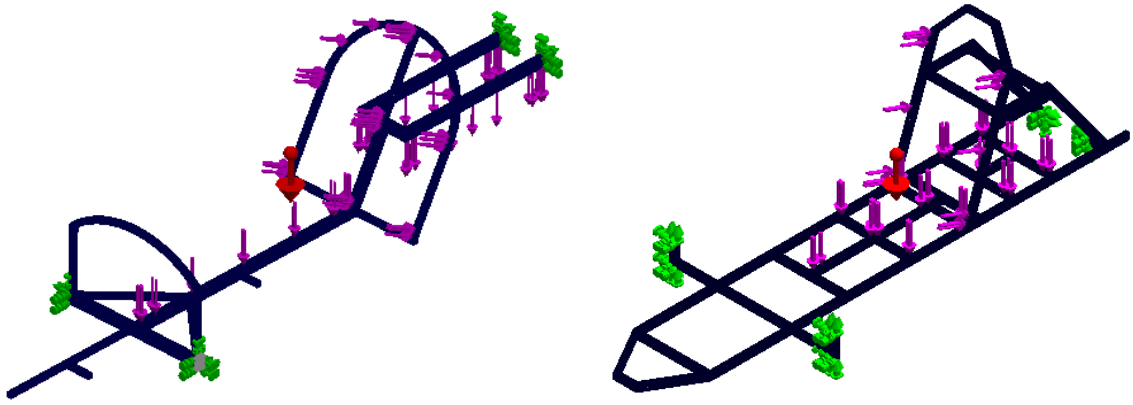

(a) First chassis (b) Second chassis

Figure 5. Finite element mesh and boundary condition setup

3. Results

A static structural finite element analysis (FEA) was performed on two chassis designs subjected to representative operational loads, namely the driver weight load and the engine weight load. Structural performance was assessed using three key responses: maximum von Mises stress, total deformation, and factor of safety (FoS). Differences in the results are influenced not only by the selected materials but also by the frame geometry, load-transfer mechanisms (load paths), and joint configurations, which govern stress concentration and overall stiffness.

3.1 Maximum von mises stress

The first chassis manufactured from AISI 1020 steel exhibited a maximum stress of 278.6 MPa at the rear frame joint near the engine mounting bracket, in shown in Figure 6a. This area is prone to high stress because engine mounts introduce a localized load transfer into the frame, often causing stress concentration at welded connections, node intersections, and abrupt stiffness transitions. In contrast, the second chassis made from Al 6061-T6 reached a maximum stress of only 61 MPa, concentrated at the rear wheel mounting region, which is also a critical zone because it carries support reactions and bending effects, in shown in Figure 6b. The comparison indicates that the second chassis produces significantly lower peak stress under the same static loading conditions. This reduction may reflect not only material behavior but also a more favorable structural layout that distributes loads more evenly and minimizes stress concentration in a single joint. Consequently, the aluminium chassis provides a larger margin against stress-driven structural failure under static loading.

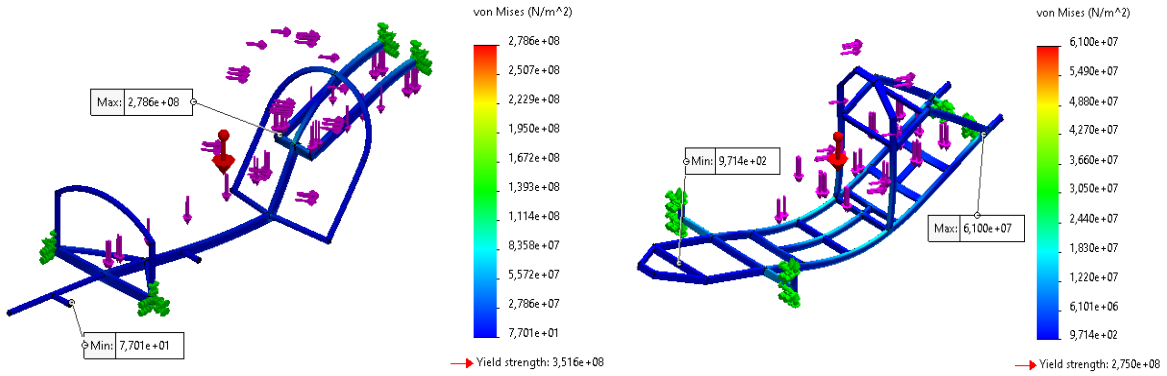

(a) First chassis made of AISI 1020 steel (b) Second chassis made of Al 6061-T6

Figure 6. Maximum von mises stress distribution under static loading

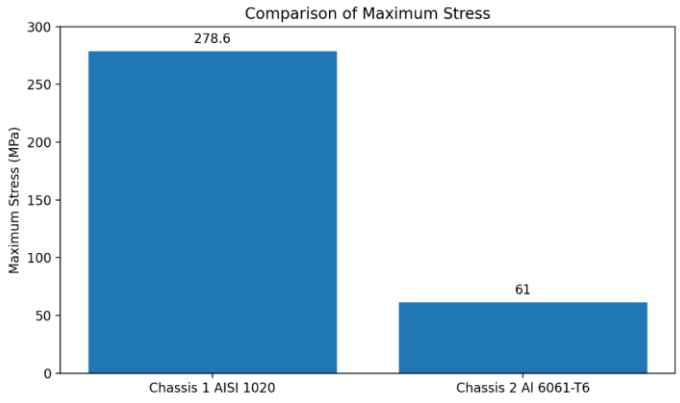

Figure 7. Comparison of maximum stress values (MPa)

Figure 7 shows that Chassis 1 (AISI 1020) experienced a much higher maximum stress (278.6 MPa) than Chassis 2 (Al 6061-T6) at 61 MPa under the same static loading. This indicates that the second chassis distributes the load more effectively and has lower stress concentrations, providing a larger safety margin against yielding compared with the first chassis.

3.2 Total deformation

The deformation results show that the first chassis (AISI 1020) experienced a maximum total deformation of 2.1 mm in Figure 8a, whereas the second chassis (Al 6061-T6) reached 3.4 mm in Figure 8b. In both configurations, the maximum deformation occurred at the driver roll bar, consistent with this region having relatively slender members and longer unsupported spans, which make it sensitive to bending. The greater deformation observed in the aluminium chassis is physically consistent because aluminium alloys generally have a lower elastic modulus than steel, leading to reduced stiffness and larger deflection under equivalent loads. Although both chassis remain within allowable deformation limits (as stated), the first chassis demonstrates higher structural stiffness, while the second chassis is more flexible under the same static load combination.

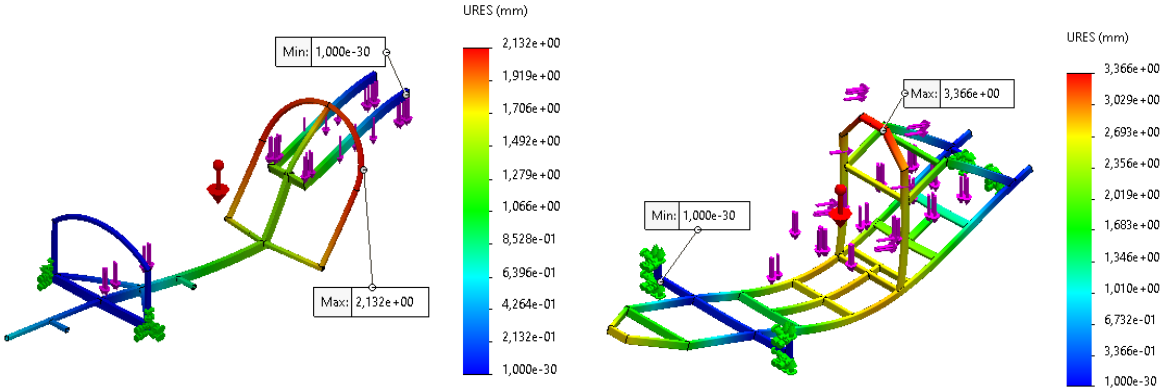

(a) First chassis made of AISI 1020 steel (b) Second chassis made of Al 6061-T6

Figure 8. Total deformation (URES) distribution under static loading

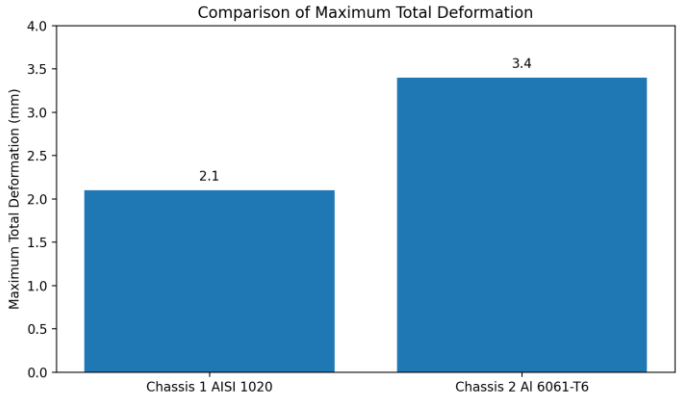

Figure 9. Comparison of maximum total deformation

Figure 9 illustrates that Chassis 2 (Al 6061-T6) experiences a higher maximum total deformation (3.4 mm) than Chassis 1 (AISI 1020) at 2.1 mm under the same static loading. This indicates that the aluminium chassis is less stiff (more flexible), while the steel chassis provides greater structural stiffness.

3.3 Factory of Safety (Fos)

The factor of safety analysis revealed that the first chassis (AISI 1020) has an FoS of 1.3, while the second chassis (Al 6061-T6) achieves an FoS of 4.5. Based on the recommended FoS range for passenger vehicle chassis structures of approximately 2.5–4, the first chassis falls below the suggested safety margin, indicating limited capacity to tolerate uncertainties such as manufacturing imperfections, weld variability, boundary-condition deviations, or additional real-world dynamic loading. Conversely, the second chassis exceeds the recommended range, suggesting that it can withstand the applied static loads with a substantial safety margin.

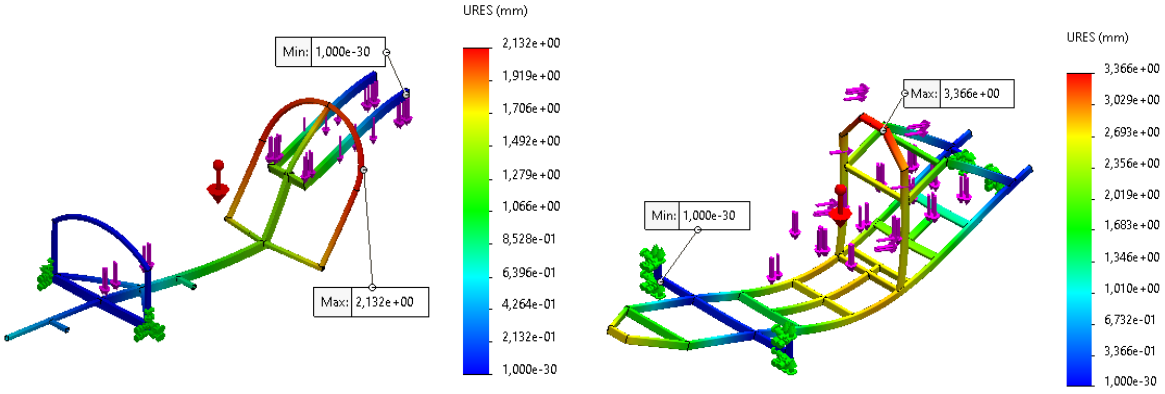

(a) First chassis made of AISI 1020 steel (b) Second chassis made of Al 6061-T6

Figure 10. Factor of safety (FoS) distribution under static loading

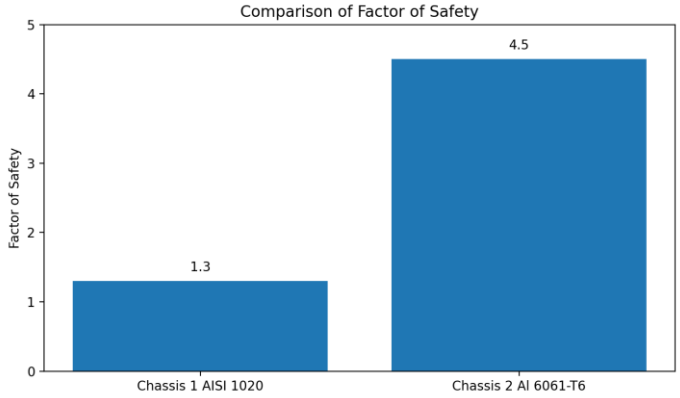

Figure 11. Comparison of Factory of Safety

Figure 11 displays that Chassis 2 (Al 6061-T6) has a much higher factor of safety (4.5) than Chassis 1 (AISI 1020) at 1.3 under the same static loading. This indicates that Chassis 2 provides a significantly larger safety margin against yielding/failure, while Chassis 1 has a relatively low safety margin and is more critical under the applied loads. Overall, the findings demonstrate a common trade-off between stiffness and static safety margin. The first chassis (AISI 1020 steel) is stiffer, as shown by its lower deformation, but it experiences a high peak stress and a low factor of safety, particularly at the engine mounting joint, indicating the need for local reinforcement or geometric optimization. In contrast, the second chassis (Al 6061-T6) shows substantially lower peak stress and a much higher FoS, indicating superior static safety performance, though it undergoes greater deformation due to its lower stiffness. Therefore, under simulated static loading conditions, the second chassis is preferable in terms of stress response and safety margin, whereas the first chassis requires design improvements at critical joints to meet the recommended safety criteria.

4. Discussion

This study compared the static structural responses of two Prototype-class chassis concepts under the same representative static loads (driver weight and engine weight), focusing on maximum von Mises stress, total deformation, and factor of safety (FoS). The outcomes highlight that chassis performance is governed by a coupled effect of material properties (yield strength and elastic modulus) and structural configuration (member layout, node connectivity, and load paths). The results also reveal a classic engineering trade-off: improving safety margin via reduced stress and increased FoS may be accompanied by increased deformation when a lower-stiffness material is used.

4.1. Interpretation of stress distribution and critical regions

The first chassis (AISI 1020) developed a maximum von Mises stress of 278.6 MPa, concentrated at the rear-frame joint near the engine mounting bracket. This behavior is consistent with structural mechanics: engine mounts introduce localized forces into a relatively small region of the frame, producing high internal bending moments and shear forces. In spaceframe-type structures, peak stresses commonly occur at node intersections, welded joints, and stiffness discontinuities, where load transfer is not purely axial but includes significant bending. Therefore, the observed stress hotspot suggests that the engine mounting region in the steel chassis acts as a stress concentrator, likely due to insufficient triangulation, abrupt geometry transitions, or a load path that funnels forces into a limited number of members. In contrast, the second chassis (Al 6061-T6) exhibited a much lower maximum stress of 61 MPa, with the hotspot located at the rear wheel mounting region. Two key interpretations can be drawn. First, the reduced peak stress indicates that the second chassis likely has a more favorable force redistribution mechanism (i.e., improved load sharing across multiple members), thereby reducing stress concentration at a single joint. Second, the shift of the critical region from the engine mount (Chassis 1) to the wheel mount (Chassis 2) implies that the second configuration transfers load differently, potentially routing a larger portion of reaction forces through the rear support structure. This finding is design-relevant: even when global performance appears improved, local details (e.g., wheel mounting nodes) may still require reinforcement because they remain structurally sensitive under combined support reactions and bending.

4.2. Deformation behavior and structural stiffness considerations

The total deformation results show that the aluminium chassis (3.4 mm) deflects more than the steel chassis (2.1 mm) under the same static load, with both reaching maximum deformation at the roll bar. This trend is expected because elastic modulus strongly governs stiffness: Al 6061-T6 (≈69 GPa) is significantly less stiff than AISI 1020 steel (≈200 GPa). As a result, for comparable structural topology and loading, aluminium structures typically exhibit higher elastic deflection. Importantly, deformation concentration at the roll bar is mechanically plausible because this region often includes curved members and longer unsupported spans, making it sensitive to bending. While the reported deformation magnitudes remain relatively small in absolute terms, the roll bar is a safety-critical element. In practical chassis design, acceptable deformation is assessed not only by magnitude but also by its potential impact on driver protection space, mounting integrity, and fatigue performance under dynamic loads. Thus, the deformation results suggest that the aluminium chassis may benefit from stiffness-oriented refinements around the cockpit (e.g., cross-bracing, additional diagonals, or reducing unsupported member lengths) to improve rigidity without substantially increasing mass.

4.3. Safety margin and implications of Factor of Safety (FoS)

A key outcome of this work is a clear contrast in factor of safety (FoS): the AISI 1020 steel chassis achieved an FoS of 1.3, while the Al 6061-T6 chassis reached 4.5 under the same static loading conditions. When benchmarked against commonly recommended FoS ranges for vehicle structures (approximately 2.5–4), the steel chassis falls below the recommended

threshold, whereas the aluminium chassis exceeds it. This indicates that the first chassis operates relatively close to yielding in its critical joint region, leaving only a limited margin to accommodate real-world uncertainties such as variability in weld quality and heat-affected zones, geometric imperfections introduced during manufacturing, deviations of actual boundary conditions from idealized simulation constraints, and additional operational loads not captured by the static model (e.g., braking/acceleration, cornering, vibration, and road-induced shocks). In contrast, the aluminium chassis provides a substantially larger safety margin under the same static scenario, implying greater robustness against these uncertainties. Nevertheless, a high static FoS should be interpreted cautiously, as it does not automatically ensure superior performance under fatigue or impact loading, where aluminium alloys, especially at welded joints, can exhibit failure characteristics different from those of steels. Therefore, although the aluminium option significantly improves the static safety margin, further verification through additional load cases and fatigue evaluation is recommended to confirm that the structural reliability is competition-ready.

4.4. Design trade-off and practical optimization direction

Taken together, the results reveal a clear and consistent trade-off between stiffness and safety margin. Chassis 1 (AISI 1020) demonstrates higher structural stiffness, as indicated by its lower deformation, but it suffers from a reduced safety margin due to pronounced stress concentration in the engine mounting region. In contrast, Chassis 2 (Al 6061-T6) provides a substantially higher safety margin, reflected in lower peak stress and a higher factor of safety, but it exhibits lower stiffness and greater deformation, particularly at the rear wheel mounting node and the roll-bar area. From a design-optimization standpoint, these outcomes suggest two practical improvement pathways. If steel remains the selected material, the main priority should be mitigating peak stress at the engine mount by introducing local reinforcements such as gussets, enhancing triangulation, and improving load-path continuity so that the structure carries loads more axially rather than through bending. Conversely, if aluminium is chosen to achieve weight reduction and a higher safety margin, the design focus should shift toward increasing cockpit rigidity, especially controlling roll-bar deformation, and reinforcing the rear wheel mounting node while preserving the mass advantage, where targeted reinforcements and topology refinement are generally more effective than uniformly increasing member size across the entire frame.

4.5. Study limitations and future work

This study employed static loads representing driver and engine masses, which is appropriate for baseline structural screening. Nevertheless, real vehicle operation involves dynamic load components (road excitation, braking/acceleration, cornering) that may increase stresses beyond static predictions and influence fatigue life. Additionally, modelling assumptions such as idealized boundary conditions and simplified load application can affect hotspot magnitude. Future work should therefore incorporate combined load cases (including torsion and lateral loads), perform mesh convergence verification, and extend the assessment to fatigue and joint/weld sensitivity, especially for aluminium structures, where the performance of the welded region is critical.

5. Conclusion

This research concludes that material selection and structural configuration significantly influence the static performance of a Prototype-class KMHE chassis under driver and engine loads. Based on the finite element analysis, the AISI 1020 steel chassis exhibited a high maximum von Mises stress of 278.6 MPa concentrated at the engine mounting joint, a maximum deformation of 2.1 mm at the roll-bar region, and a low factor of safety of 1.3, indicating that the structure operates close to yielding and does not meet recommended safety margins for vehicle structures. In contrast, the Al 6061-T6 chassis produced a much lower peak stress of 61 MPa located at the rear wheel mounting region and achieved a higher factor of safety of 4.5, demonstrating a substantially greater static safety margin; however, it showed

a higher deformation of 3.4 mm due to the lower elastic modulus of aluminium, reflecting reduced global stiffness. Overall, the findings confirm a clear trade-off between stiffness and safety margin: the steel chassis is stiffer but structurally more critical and requires reinforcement and load-path optimization, particularly at the engine mount, while the aluminium chassis is statically safer but should be improved through targeted stiffening in the cockpit (roll-bar) and reinforcement at the rear wheel mounting node. Future validation should include dynamic load cases and fatigue assessment to ensure competition-ready reliability, especially for welded joints.

Author's Declaration

Author contribution

Muhammad Fadil Andira: Conceptualization, Methodology, Investigation, Formal Analysis, Writing–Original Draft, Writing–Review & Editing, Visualization, Supervision, Project Administration. **Wanda Afnison:** Investigation, Data Curation, Software, Validation, Writing–Review & Editing, Visualization. **Waskito:** Methodology, Software, Validation, Formal Analysis, Writing–Review & Editing. **Delima Yanti Sari:** Supervision, Validation, Writing–Review & Editing, Resources.

Funding statement

This research received no specific grant from any funding agency in the public, commercial, or not-for-profit sectors.

Acknowledgement

The authors gratefully acknowledge the support and contributions provided by the lecturers of the Mechanical Engineering Department, Faculty of Engineering, Universitas Negeri Padang, Indonesia, for their guidance and facilitation throughout the completion of this research.

Competing interest

The authors declare that there are no competing interests related to the research or publication of this article.

Ethical clearance

This research does not involve humans as subjects.

Data availability

No applicable.

AI statement

This research was written entirely in its original form, and no data were generated using generative AI. However, Grammarly was used to improve the manuscript's readability and clarity.

Publisher's and Journal's Note

Researcher and Lecturer Society as the publisher, and the editor of Journal of Engineering Researcher and Lecturer state that there is no conflict of interest towards this article publication.

References

Ambaw, A., Mukama, M., Fadiji, T., & Linus, U. (2022). Fresh fruit packaging design verification through virtual prototyping technique. *Food Packaging and Shelf Life*, *32*, 100858. https://doi.org/10.1016/j.fpsl.2022.100858

Anil, C. K., Srinivas, S., Manjunath, M., Satish, M., & Khot, M. B. (2025). Selection of Materials , Design and Analysis of FSAE Chassis for Different Engineering Application- A Comprehensive Review. *International Journal of Automotive Science And Technology*, *9*(1), 136–157. https://doi.org/10.30939/ijastech..1574611

Brown, N. E., Rojas, J. F., Goberville, N. A., Alzubi, H., Alrousan, Q., Wang, C. R., Huff, S., Rios-torres, J., Ekti, A. R., Laclair, T. J., Meyer, R., & Asher, Z. D. (2022). Development of an Energy Efficient and Cost Effective Autonomous Vehicle Research Platform. *Sensors*, *22*, 1–30. https://doi.org/10.3390/s22165999

Cornet, A., Heuss, R., Schaufuss, P., & Tschiesner, A. (2023). A road map for Europe's automotive industry. In *Automotive & Assembly Practice* (Issue August, pp. 1–14). https://www.mckinsey.com/industries/automotive-and-assembly/our-insights/a-road-map-for-europes-automotive-industry#/

Czerwinski, F. (2021). Current trends in automotive lightweighting strategies and materials. *Materials*, *14*(21), 1–27. https://doi.org/10.3390/ma14216631

Demiral, M. (2025). Strength in Adhesion: A Multi-Mechanics Review Covering Tensile, Shear, Fracture, Fatigue, Creep, and Impact Behavior of Polymer Bonding in Composites. *Polymers*, *17*, 1–47. https://doi.org/10.3390/polym17192600

Ding, R., Qi, X., Chen, X., Mei, Y., & Li, A. (2025). The Current Development Status of Agricultural Machinery Chassis in Hilly and Mountainous Regions. *Applied Sciences*, *15*, 1–40. https://doi.org/10.3390/app15137505

Gadola, M., Chindamo, D., Legnani, G., & Comini, M. (2019). Teaching automotive suspension design to engineering students: Bridging the gap between CAD and CAE tools through an integrated approach. *International Journal of Mechanical Engineering Education*, *47*(1), 23–43. https://doi.org/10.1177/0306419018762803

Golinska-Dawson, P., & Sethanan, K. (2023). Sustainable Urban Freight for Energy-Efficient Smart Cities—Systematic Literature Review. *Energies*, *16*(2617), 1–28. https://doi.org/10.3390/en16062617

Heidari, A., Amiri, Z., Ali, M., Jamali, J., & Jafari, N. (2024). Assessment of reliability and availability of wireless sensor networks in industrial applications by considering permanent faults. *Concurrency and Computation: Practice and Experience*, *36*(27), 1–21. https://doi.org/10.1002/cpe.8252

Kabashi, N., Muhaxheri, M., Krasniqi, E., Murati, Y., & Latif, F. (2025). Advancements in Fiber-Reinforced Polymer (FRP) Retrofitting Techniques for Seismic Resilience of Reinforced Concrete Structures. *Buildings*, *15*, 1–23. https://doi.org/10.3390/buildings15040587

Lagaros, N. D., Plevris, V., & Ath, N. (2022). The Mosaic of Metaheuristic Algorithms in Structural Optimization. *Archives of Computational Methods in Engineering*, 1–36. https://doi.org/10.1007/s11831-022-09773-0

Laveneziana, L., Marin, A. L., O'Brien, D., Prussi, M., & Fontaras, G. (2025). A science-based approach to classifying light vehicles in Europe: methodology and case studies. *Scientific Reports*, *15*(9099), 1–28. https://doi.org/10.1038/s41598-025-90625-9

Liu, R., Chen, W., & Zhao, J. (2024). A Review on Factors Affecting the Mechanical Properties of Additively-Manufactured Lattice Structures. *Journal of Materials Engineering and Performance*, *33*(10), 4685–4711. https://doi.org/10.1007/s11665-023-08423-1

Muayad, H., Raffaele, C., Marco, D., Hamed, F., & Rad, M. M. (2025). Thermo-mechanical reliability-based topology optimization for imperfect elasto-plastic materials. *International Journal of Mechanics and Materials in Design*, *21*(6), 1755–1776. https://doi.org/10.1007/s10999-025-09799-9

Nozari, H., Nassar, S., & Szmelter-jarosz, A. (2025). Fuzzy Multi-Objective Optimization Model for Resilient Supply Chain Financing Based on Blockchain and IoT. *Digital*, *5*, 1–23. https://doi.org/10.3390/digital5030032

Pign`eres, E., Buche, P., Dole, P., Gaucel, S., Angellier-Coussy, H., Gontard, N., Coffigniez, F., & Guillard, V. (2025). A requirement-driven approach to design food packaging: A new

decision support system relying on structured database. *Innovative Food Science and Emerging Technologies*, *104*, 104096. https://doi.org/10.1016/j.ifset.2025.104096

Quang, N. T. (2019). Finite Element Analysis in Automobile Chassis Design. *Applied Mechanics and Materials*, *889*, 461–468. https://doi.org/10.4028/www.scientific.net/AMM.889.461

Razmjoo, A., Nezhad, M. M., Kaigutha, L. G., Marzband, M., Mirjalili, S., Pazhoohesh, M., Memon, S., Ehyaei, M. A., & Piras, G. (2021). Investigating Smart City Development Based on Green Buildings, Electrical Vehicles and Feasible Indicators. *Sustainability (Switzerland)*, *13*, 1–14. https://doi.org/10.3390/su13147808

Sarvestani, H. Y., Patel, J., Azad, E., & Ashrafi, B. (2025). Flexible multilayered ceramics: Engineering strength and resilience. *Journal of Science: Advanced Materials and Devices*, *10*(2), 100874. https://doi.org/10.1016/j.jsamd.2025.100874

Silva, C. J. G., Lopes, R. F. F., Domingues, T. M. R. M., Parente, M. P. L., & Moreira, P. M. G. P. (2024). Crashworthiness topology optimisation of a crash box to improve passive safety during a frontal impact. *Structural and Multidisciplinary Optimization*, *68*(3), 1–24. https://doi.org/10.1007/s00158-024-03924-6

Tuninetti, V., Narayan, S., Ríos, I., Menacer, B., Valle, R., Al-lehaibi, M., Kaisan, M. U., Samuel, J., Oñate, A., Pincheira, G., & Mertens, A. (2025). Biomimetic Lattice Structures Design andManufacturing for High Stress, Deformation, and Energy Absorption Performance. *Biomimetics*, *10*(458), 1–37. https://doi.org/10.3390/biomimetics10070458

Zamzam, O., Ramzy, A. A., Abdelaziz, M., El-wahab, A. A. A., & Elnady, T. (2025). Structural performance evaluation of electric vehicle chassis under static and dynamic loads. *Scientific Reports*, *15*, 1–20. https://doi.org/10.1038/s41598-025-86924-w

Zhu, X., Cai, L., Lai, P., Wang, X., & Ma, F. (2023). Evolution, Challenges, and Opportunities of Transportation Methods in the Last-Mile Delivery Process. *Systems*, *11*(509), 1–28. https://doi.org/10.3390/systems11100509